PNAS

Main Manuscript for

Design of a Light and Ca^{2+} Switchable Organic-Peptide Hybrid

Zinah Hilal Khaleel[1,2,3,+], Young Hyun No[1,3,+], Nam Hyeong Kim[1,3,4,+], Do Hyun Bae[2,5], Yibing Wu[4], Suhyeon Kim[1,3], Hojae Choi[1,3], Da Eun Lee[6], Se Yun Jeong[6], Yoon-Joo Ko[7], Seong-Gi Kim[2,5], Minah Suh[2,5,8], Jin-Chul Kim[9,10,*], William F. DeGrado[4,*], Ki Hyun Kim[6,*], Yong Ho Kim[1,2,3,5,8,11,*]

[1]SKKU Advanced Institute of Nanotechnology (SAINT), Sungkyunkwan University, Suwon 16419, Republic of Korea

[2]Center for Neuroscience Imaging Research, Institute for Basic Science (IBS), Suwon 16419, Republic of Korea

[3]Department of Nano Science and Technology, Sungkyunkwan University, Suwon 16419, Republic of Korea

[4]Department of Pharmaceutical Chemistry and the Cardiovascular Research Institute, University of California at San Francisco, California 94158, United States

[5]Department of Biomedical Engineering, Sungkyunkwan University, Suwon 16419, Republic of Korea

[6]School of Pharmacy, Sungkyunkwan University, Suwon 16419, Republic of Korea

[7]Laboratory of Nuclear Magnetic Resonance, National Center for Inter-University Research Facilities (NCIRF), Seoul National University, Seoul 08826, Republic of Korea

[8]IMNEWRUN Inc., Suwon 16419, Republic of Korea

[9]Natural Products Research Center, Korea Institute of Science and Technology (KIST), Gangneung 25451, Republic of Korea

[10]Division of Bio-Medical Science & Technology, KIST school, University of Science and Technology (UST), Seoul 02792, Republic of Korea

[11]Department of Nano Engineering, Sungkyunkwan University, Suwon 16419, Republic of Korea

* To whom correspondence may be addressed.

Email: jckim@kist.re.kr, william.degrado@ucsf.edu, khkim83@skku.edu and yhkim94@skku.edu

Author Contributions: Z.H.K., Y.H.N. and N.H.K. contributed equally to this work. Z.H.K., and Y.H.K. conceptualized and designed the study; Z.H.K., and Y.H.K. supervised the experiment; Z.H.K., W.F.D. and Y.H.K. wrote the manuscript; Z.H.K. synthesized peptide and analyzed experimental properties of CaBS; Z.H.K., Y.W., D.E.L. and K.H.K. measured and analyzed NMR data; H.C. worked on Rosetta, Y.H.N. analyzed generated NMR structure by MD simulation. N.H.K., J.C.K., K.H.K., W.F.D. and Y.H.K. contributed to the discussion and revision of the draft. All authors have given approval to the final version of the manuscript.

Competing Interest Statement: We filed the patent in Korea (Application No. 10-2022-0167085).

Classification: Biological sciences

Keywords: metalloprotein, peptide–organic hybrid, photoswitchable, spiropyran/merocyanine, bioinorganic chemistry.

This PDF file includes:

Main Text
Figures 1 to 5
Schemes 1 to 2

Abstract

The design of organic-peptide hybrids has the potential to combine our vast knowledge of protein design with small molecule engineering to create hybrid structures with complex functions. Here we describe the computational design of a photoswitchable Ca^{2+}-binding organic-peptide hybrid. The designed molecule, designated Ca^{2+}-binding switch (CaBS), combines an EF-hand motif from classical Ca^{2+}-binding proteins such as calmodulin with a photo-switchable group that can be reversibly isomerized between a spiropyran (SP) and merocyanine (MC) state in response to different wavelengths of light. The MC/SP group acts both as a photo-switch as well as an optical sensor of Ca^{2+} binding. Photoconversion of the SP to the corresponding MC unmasks an acidic phenol, which CaBS uses as an integral part of both its Ca^{2+}-binding site as well as its tertiary and quaternary structure. By design, the SP state of CaBS is monomeric, while the Ca^{2+}-bound form of the MC state is an obligate dimer, with two Ca^{2+}-binding sites formed at the interface of a domain-swapped dimer. Thus, light and Ca^{2+} were expected to serve as an "AND gate" that powers a change in backbone structure/dynamics, oligomerization state, and fluorescence properties of the designed molecule. CaBS was designed using Rosetta and molecular dynamics simulations, and experimentally characterized by NMR, isothermal titration calorimetry (ITC), and optical titrations. These data illustrate the potential of combining small molecule engineering with *de novo* protein design to develop sensors whose conformation, association state and optical properties respond to multiple environmental cues.

Significance Statement

This article details the creation of photoswitchable organic-peptide hybrids that self-associate into Ca^{2+}-binding dimers when exposed to specific light wavelengths. This research highlights the potential of photoswitchable compounds to regulate complex equilibria, enabling the design of photoactive systems. These findings could lead to new applications in various fields, demonstrating the ability to control protein behavior with light and calcium.

Introduction

Metal ions have gained recognition as essential elements in biological systems, owing to their multifaceted roles in processes such as photosynthesis,(1, 2) electron transfer,(3) transport, signal transduction,(4) and catalysis.(5) To carry out these diverse functions, metals require specific binding motifs that can accommodate precise redox states and geometric arrangements. With the advent of metalloprotein engineering and *de novo* protein design, it has become increasingly feasible to uncover intricate structure-function relationships within naturally occurring metalloproteins and tailor the properties of both natural and novel metalloproteins for specific applications.(6-11) Nevertheless, the design of metalloproteins remains challenging, as it demands a complex interaction network with exact coordination numbers, along with second- and third-shell hydrogen-bonded interactions, to stabilize the binding site — a critical factor in preserving their function.

To expand the repertoire of structural motifs for metal recognition and actively regulate the function of metalloproteins, the integration of organic-peptide hybrid materials has gained significant attention. The integration of peptides and organic components has the potential to combine the chemical properties of small molecule ligands with the specificity and conformational properties of natural proteins. Porphyrins, for example, mediate metal binding when incorporated into helical bundles, thereby facilitating catalytic and redox activities.(12, 13) Additionally, organic moieties offer the potential for introducing novel functionalities within relatively compact, tunable packages, including photocatalytic, photoswitchable, and photo-redox activities.(14-24)

Here, we computationally design a calcium-binding switchable peptide-organic hybrid whose conformation and oligomerization state can be controlled by the combined stimuli of light and Ca^{2+} binding. These studies build on previous work on the design of photoswitches in proteins involving diazobenzenes and photoactive LOV domains, which generally relied on a single stimulus to switch conformation.(25-37) As the light-switchable group, we used a spiropyran (SP) — a photoswitchable chromic molecule — that can be photo-isomerized between two forms: from ring-closed form SP to the ring-open form merocyanine (MC). The ring-opened MC form is converted to the SP by irradiation at 365 nm, while the reverse reaction is promoted by visible light in the range of 400-600 nm. (Scheme 1). Thermal isomerization between the two is slow, allowing photo-control of both states. The presence of a negatively charged oxygen (O-) atom in the MC structure allows it to coordinate metal ions, which also leads to a shift in the MC absorbance upon binding to the target (Scheme 1). We integrate this photo-switchable moiety into a peptide framework to engineer a light-triggered sensor with finely tuned metal-binding properties. Moreover, the metal-bound state was designed to form an obligate dimer by building across the interface of a domain-swapped dimer. Our designed calcium-binding switchable peptides demonstrate the remarkable control that can be achieved by combining organic and peptidic elements: upon photoconversion, CaBS undergoes a dramatic change in backbone conformation, association state, UV/visible absorption and fluorescence, and Ca^{2+} affinity. Moreover, CaBS shows high specificity for Ca^{2+} over other divalent metal ions, showing the promise of our approach for design of sensitive and selective photoswitchable metal ion sensors.(23, 31, 38-42)

Results and Discussion

Design strategy

The MC used in this work features a phenolate, which associates weakly to divalent cations.(43-45) However, more specific recognition of metal ions using this derivative has not been reported to the best of our knowledge. To enhance metal ion selectivity, we turned to the EF-hand family of Ca^{2+}-binding peptides, known for their classic motif comprising a short Ca^{2+} binding loop with multiple carboxylate and carbonyl ligands.(46-49) The CaBS was designed by combining the core of the Ca^{2+} binding site of an EF-hand from calmodulin(50) (sequence number from 20 to 31, sequence DKDGDGTITTKE) and the photo-switchable metal-binding ligand, MC (Figure 1). The calcium in the EF-hand is coordinated by seven oxygen ligands: one chelating carboxylate, three monovalent carboxylates, one backbone carbonyl and one water. To convert this peptide into a switchable CaBS, the peptide was truncated prior to the Glu31 ligand, and the Ca^{2+}-binding MC was then grafted onto the N-terminus of the peptide. Due to its elongated nature, the MC projected away from the Ca^{2+}-binding site (Figure 1); to solve this problem, we considered a C2-symmetric dimer, where the MC oxygen ligand appeared ideally positioned to complete the coordination sphere of a symmetry-related monomer, creating a domain-swapped dimer (Figure 1 and S1). Thus, the chelating Glu31 was removed and replaced with a monovalent phenolate of the MC. We then utilize Rosetta SetupMetalsMover(51-53) (Supplementary information) to optimize the geometry of the dimeric complex. During optimization, Asp22 (which was a monovalent ligand in the native protein) transitioned from a monovalent to a chelating orientation by a carboxylate shift(54) increasing the interaction with the Ca^{2+} ion (Figure S1A and B). We evaluated the geometrical favourability of the optimized coordination geometry by varying the angle between two vectors, one representing the direction of the elongated MC molecule (SP) and the other for the peptide. The angle between these vectors served as a convenient collective variable for each dimer, guiding in the formation of a C2-symmetric dimer (refer to Figure S1C and D). Additionally, the 7th position of the calcium-binding EF hand appeared well-suited for forming a hydrophobic interaction with the apolar MC

group of a symmetry-related monomer (Figure S2A). We therefore explored positioning hydrophobic residues, namely V, T, F, or Y at this position. These peptides are designated as CaBS.V, CaBS.T, CaBS.F, and CaBS.Y, respectively.

Molecular dynamics (MD) simulation

To evaluate the conformational stability and Ca^{2+} ion binding of the designed candidates, 500 ns MD simulations were carried out at 298 K for each construct, using the designed structures as the initial models. Among the designed candidates, the CaBS.F dimer exhibited the lowest Ca^{2+} binding energy (Figure 2A) and was the sole candidate that maintained a C2-symmetric dimer (Figure 2B). These findings suggest that phenylalanine in CaBS.F plays a crucial role in hydrophobically stabilizing the C2-symmetric dimer structure and facilitating Ca^{2+} binding via hydrophobic interactions between the apolar MC group and the peptide.

To assess the Ca^{2+} binding coordination geometry in CaBS.F, ligating atoms within 2.6 Å of the Ca^{2+}: we monitored the distance between Ca^{2+} and its intended ligands: the carbonyl of Phe7 carbonyl oxygen, MC phenolate, and carboxylates of Asp1, Asp3, and Asp5, as well as solvent water during the last 100 ns MD simulation. Throughout the simulations, the Ca^{2+} bound form of CaBS.F retained the desired metal ion ligation, and the overall structure (Figure 2C). The mean calcium binding distance was 2.3 ± 0.1 Å, which is an acceptable distance for binding to Ca^{2+}. Furthermore, the total mean coordination number was 6.7, well within the range observed for Ca^{2+} chelates (Figure S2B and C). Additionally, removal of Ca^{2+} from the Ca^{2+}-bound dimer resulted in rapid dissociation within 5 ns of the MD simulation; at later times the two monomers continued to diffuse away from one another, reaching a distance of over 40 Å after 150 ns of simulation (Figure 2D and S3). This finding suggested that Ca^{2+} was required to maintain a stable folded dimeric structure. Overall, MD simulation results demonstrated that of the CaBS evaluated, CaBS.F was uniquely predicted to bind Ca^{2+} in the predicted geometry when in the light-triggered MC state (Movie S1 and Movie S2).

Calcium binding, selectivity and photoactivity

The designed spiropyran peptides (CaBS.V, CaBS.T, CaBS.F, and CaBS.Y) were synthesized (Scheme 2), starting with a 4-carboxy derivative of the SP group. With the CaBS in hand, we first examined their photochemical properties in the absence of Ca^{2+}. Under broad-band UV irradiation, the SP form converted to the MC (Figure S4), the time course reached a maximum absorbance after 120 sec, indicating that it had reached photosaturation.(55) The resulting MC form was thermally stable at room temperature for 5 min in the dark but could be readily reversed to the SP by irradiation under visible light.

We next assessed the metal binding properties of the SP and photoconverted MC forms of the CaBS candidates. Notably, the CaBS.F peptide showed robust absorbance bands in phosaphate-buffered saline (PBS) at 410 nm in the presence of 1.0 equivalent of Ca^{2+}, whereas equivalent concentrations of Zn^{2+}, Na^{+}, Cu^{2+}, Co^{2+}, Mn^{2+}, and Mg^{2+} did not produce similar absorbance. We also examined La^{3+} which is a commonly used substitute for Ca^{2+}. Lanthanides have similar van der waals radii as Ca^{2+}, but 3+ charge, which frequently leads to increased affinity (56-59). Indeed, La^{3+} exhibited a similar absorbance pattern to Ca^{2+}. (Figure 3A), these trends were also clearly apparent upon visual inspection of the solutions (Figure S5), in contrast to other variants that showed little to no spectral changes (Figure S6). Furthermore, a titration of Ca^{2+} into CaBS.F showed an increase in the 410 nm band, reaching a maximum near 1.0 equivalent of metal ion as expected for the designed complex of 2 Ca^{2+} per dimer (Figure 3B).

The changes in absorption were also reflected in changes in the fluorescent emission spectrum (Figure 3C). Peptide CaBS.F showed little fluorescence in the absence of Ca^{2+}. However, upon

addition of Ca the fluorescence at 497 nm increased 14-fold with increasing concentration of Ca^{2+} up to 1.2 equivalents. Thus, peptide CaBS.F serves as an efficient turn-on fluorescent sensor for physiologically relevant concentrations of Ca^{2+}. Moreover, Ca^{2+} binding could be reversibly turned on and off by using visible (to induce the MC form) and UV light (to relax the structure to the SP form); this reversibility could be realized in multiple cycles without any intensity loss 10 cycles (Figure 3E).

To confirm the spectral titrations, the binding affinity of CaBS.F for Ca^{2+} was determined using isothermal titration calorimetry (ITC). Saturable binding curves for CaBS.F were seen with a stoichiometry of one Ca^{2+}/peptide. Therefore, the data were analyzed according to a sequential binding model, which assumes ligands bind to the receptor in a stepwise ordered manner (N = 2), K_D = 0.713 μM and 1:1 stoichiometry (Figure S7A). This K_D value is consistent with a titration curve obtained from UV/visible spectroscopy of CaBS.F (Figure 3D, S8 and S9). Showing the selectivity for Ca^{2+}, a similar ITC titration of CaBS.F with Zn^{2+}, Na^{+}, Cu^{2+}, Co^{2+}, Mn^{2+}, and Mg^{2+} showed no excess heat generation over the same concentration range while ITC titrations with La^{3+} demonstrated binding with measurable heat of interaction, supporting our claim of CaBS.F's selectivity towards Ca^{2+} (Figure S7, S8). These findings provide experimental support for the designs and MD simulations, which predicted the superior stability of CaBS.F – calcium complex relative to the others.

NMR investigation of the calcium binding sites and domain swapped dimer structure

We further evaluated the binding of Ca^{2+} of CaBS.F and the association state of the complex using the nuclear magnetic resonance (NMR) spectrum of CaBS.F before and after Ca^{2+} addition (Figure 4, S11-23 and Table S1). All experiments in this section were conducted on the MC form of CaBS.F that is capable of binding to Ca^{2+}. The HMBC spectrum showed clear changes in the chemical shifts of residues associated with ligation of the metal ion, including Asp1, Asp3 and/ Asp5. Moreover, changes of the chemical shifts were associated with Phe7 and C-14 of the MC (Figure 4B and 4C), which are centrally located in the apolar interface in the designed model of the structure (Table S1, Figure S19). The stoichiometry of CaBS.F was further probed using a Job analysis,(63) which showed a maximum value at 0.5 mole fraction of CaBS.F in a Job plot. This value indicates a 1:1 stoichiometry, which is consistent with two Ca^{2+} per CaBS.F (Figure 4D and S20, Table S2).

We next evaluated the Ca^{2+}-induced association of CaBS.F by measuring its diffusion coefficient (D) using DOSY NMR. A progressive change to lower D was clearly observed as the calcium ion concentration increased (Figure 4E and Table S3). The decreasing D-values indicate an increase in molecular size.(64) The D value decreased up to 1 equivalent of calcium ions, beyond which there was no significant change in calcium ion concentration. The observed change in D was consistent with an increase in the CaBS.F stoichiometry from monomer to dimer, as expected from the MD simulations. We further confirmed the dimerization behavior in the presence of Ca^{2+} by using size exclusion chromatography (SEC).(65) In the absence of Ca^{2+}, CaBS.F eluted at a volume expected for the monomer; however, as increasing concentrations of Ca^{2+} were added, the mixture gradually changed to a dimer, with 70–80 % of the mixture being dimeric in the presence of 1.0 equivalent of Ca^{2+} (Figure 4F). However, when other variants of CaBS (CaBS.T, CaBS.V, CaBS.Y) were examined under the same conditions, no dimeric chromatographic shift was observed in the presence of 1.5 equivalent of calcium ions (Figure S10).

To probe the conformation of the dimer, we employed a selective Nuclear Overhauser Effect (NOE) method to target specific positions in the molecular structure. 1D NOE was measured between the phenyl ring of Phe7 and H-19/H-20 of MC, when the H-5/H-9 and H-6/H-8 of Phe7

were irradiated, the peaks for H-19/H-20 of MC appeared, and conversely, when the H-19/H-20 protons of MC were irradiated, the peaks for H-5/H-9 and H-6/H-8 of Phe7 were observed. In addition, once the H-3 of Phe7 was irradiated, the peaks for H-16/H-17 of MC appeared, and the reverse case was also observed (Figure S25-28). This finding strongly supports the domain-swapped dimer, the observed NOEs indicate the distance between the phenyl ring of Phe7 and H-19/H-20 of MC as well as that between the H-3 of Phe7 and H-16 (or H-17) of MC were less than 5 Å.

To obtain additional structural insight of CaBS.F-Ca^{2+} ensembles, MD simulations were carried out with restraining NOE-derived interproton distances that were calculated using PANIC analysis from ROESY (Figure S22-23 and Table S4).(66) The designated structure was simulated for 300 ns with harmonic distance restraints to apply NOE-derived experimental distance and 30,000 structures were extracted from the trajectories at 10 ps intervals for cluster analysis. Five distinct structures were identified; the first cluster clearly dominates, accounting for 99.32 % of the entire trajectory data (Figure 5B). This provides strong evidence that the peptide is uniquely folded in the desired conformation. The representative structure from this dominant cluster was then compared to the originally designed model (Figure 5A and S24). The analysis revealed that the structures were highly similar, exhibiting an RMSD value of 1.97 Å. The NOE derived structure closely resembled the designed model in terms of coordination geometry, with all 7 intended coordination bonds present (Figure 5B). Additionally, the hydrophobic interaction regions were sufficiently close to stabilize the swapped dimer structure as intended (Figure 5C). The NMR-generated structure provides compelling evidence that the designed CaBS.F exhibits high accuracy in its unique swapped dimeric structure, and well-fitted calcium binding geometry.

Conclusion

In conclusion, we designed a calcium binding switchable peptide by integrating a peptide and organic moiety, resulting in a peptide whose conformation, association state and metal ion-binding properties could be switched on and off in response to light. There is considerable interest in the design of proteins that respond to stimuli such as light absorption or the binding of metal ions to effect changes in conformation and assembly. Here we describe a strategy for design of peptides and proteins that can be optically switched to an isomeric form that is capable of binding Ca^{2+} with concomitant changes in conformation and association state. Moreover, the fluorescence is greatly enhanced upon Ca^{2+}-binding, illustrating the potential for this approach to yield highly specific optical metal ion sensors. These approaches provide the potential of combining small molecule engineering with *de novo* protein design for the creation of molecules that respond to multiple stimuli.

Materials and Methods

Materials

All chemicals and solvents were purchased from commercial suppliers and used directly without further purification unless stated otherwise. The H-rink amide resin was purchased from PCAS. Piperidine was purchased from Alfa aesar. Ethyl Cyano (hydroxyimmino) acetate (oxyma) was purchased from TCI, Diisopropylcarbodiimide (DIC) was purchased from Sigma-Aldrich, triisopropylsilane (TIS), phosphate buffer (IX), trifluoroacetic acid (TFA) was purchased from Daejung. Dichloromethane (DCM) and Dimethylformamide (DMF), Acetonitrile (CAN), Triethylamine acetate (TEAA) and ether were purchased from Daejung and SAMCHUN. HPLC (waters) was used with a reverse-phase chromatography column (C18, 19 mm x 250 mm), gradient with different initial ratio between solvent (A 90 % and B 10 %). Molecular mass was confirmed by matrix-assisted in desorption/ionization time of flight, MALDI-TOF (High Performance mk: TOF system: autoflex max). Absorption and emission spectra were recorded using Varian Cary 500 and Varian Cary Eclipse, respectively. The UV (365 nm, 2.6 $W \cdot cm^{-2}$) and light-emitting diode (LED) lamps (360 nm, 150 $mW \cdot cm^{-2}$) were used as light sources for UV and visible light irradiation. ITC measurement was performed with MicroCal iTC200 in Shanghai Institutes for Biological Sciences. FPLC was measured on AKTA FPLC, NMR spectra were recorded using a Bruker AVANCE III spectrometer (Bruker Corporation). High-resolution-electrospray ionization (HR-ESI) mass spectra were recorded using an Agilent 1290 Infinity II system equipped with a 6545 LC/Q-TOF mass spectrometer (Agilent Technologies).

Protein Design

Merocyanine (MC) structure was generated on maestro with structure minimization and the param file was generated on Rosetta (see the supporting information script). Coordinates for the calmodulin motif (residues 20-26) were extracted from the crystal structure (PDB: 1CLL), maintaining their four coordinate bonds with Ca^{2+}. The MC was then added to the C-terminus via an amide bond. After generating the second motif through domain swapping with C2 symmetry, the optimal orientation for coordinate bonds was identified using a Monte Carlo simulated annealing protocol implemented with the 'SetupMetalMover' and 'FastRelax' movers in RosettaScript. The RosettaScripts used are provided at the end of the Supporting Information.

Molecular dynamics simulation

The MD simulations were carried out with the structures of the 4 MC-peptide candidates designed by Rosetta considering the coordination geometry of Ca^{2+} ion binding. The equilibrium MD simulations were performed with NAMD package with CHARMM36 force field(67) to observe the structural stability of design candidates. The force field parameters of MC were created with CHARMM-GUI input generator.(68) After energy minimization during 20 ps at 300 K, the following equilibrium simulations were carried out using an NPT ensemble at 300 K for 500 ns. The binding energy between two monomers was calculated based on the molecular mechanics-Poisson-Boltzmann surface area (MM-PBSA) method.(69)

Synthesis of 1-ethyl-3,3-dimethyl-2-methyleneindoline

2,3,3-Trimethyl-3H-indole (1 ml, 6.9 mmol) was dissolved in MeCN (0.5 ml). Methyl hypoiodite (2 ml, 12 mmol) was then added, and the reaction mixture was refluxed for 48 hours under nitrogen gas. After cooling, the solid was filtered off, washed with MeCN and $CHCl_3$, then dried under vacuum, yielding a pink powder.^{1}H NMR $CDCl_3$: δ1.67 (1H, s), 2.10 (6H, s), 2.48 (2H, s), 3.65 (3H, s), 7.50 7.67 (3H, 7.56 (td, J =7.9, 1.4 Hz), 7.57 (ddd, J =7.9, 1.4, 0.4 Hz), 7.61 (td, J = 7.9, 1.6 Hz), 8.09 (1H, ddd, J = 7.9, 1.6, 0.4 Hz) 91 % yield. Then to remove the iodide ion, the final product was stirred in a 0.5 M NaOH and $CHCl_3$ mixture (50:50 v/v) for 30 mins. The product

was then extracted with $CHCl_3$ and deionized waters and dried using vacuum evaporator, resulting in a purple liquid-like product. ^{1}H NMR $CDCl_3$: δ1.40 (6H, s), 3.70 (3H, s), 4.99 (1H, d, J = 1.7 Hz), 5.21 (1H, d, J= 1.7 Hz), 6.73 (1H, ddd, J=80.0, 1.3, 0.6 Hz), 6.98, 7.19 (2H, 7.04 (ddd, J =84, 1.3, 0.6 Hz), 7.12 (ddd, J = 8.0, 7.5, 1.3 Hz)), 7.27 (1H, ddd, J = 8.4, 7.5, 1.3 Hz) 80 % yield (Figure S29).

Synthesis of 1'-ethyl-3',3'-dimethylspiro[chromene-2,2'-indoline]-6-carboxylic acid

One equivalent of 1-ethyl-3,3-dimethyl-2-methyleneindoline was dissolved in 2 mL of ethanol, and 1 equivalent of 4-formyl-3-hydroxybenzoic acid was added. The reaction mixture was stirred under reflux for 12 hours. Afterward, the solvent was removed using a vacuum evaporator, and the product was purified through silica gel column chromatography (100% DCM). The collected product was then evaporated under reduced pressure, yielding a red to purple crystalline product. ^{1}H NMR $CDCl_3$: δ 1.27, 1.37 (6H, 1.329 s), 1.32 (s), 3.56 (3H, s), 6.38 (1H, d, J=9.7 Hz), 6.69, 6.83 (2H, 6.67(ddd, J = 7.7, 75, 1.1H), 6.75 (ddd, J = 7.7, 75, 1.1H)), 7.02-7.27 (4H, 7.09 (dd, J =8.4, 0.5 Hz), 7.09 (ddd, J =.7, 1.5, 0.4 Hz), 7.17 (d, J =9.7 Hz), 7.20 (ddd, J =7.8, 7.5, 1.5 Hz)), 7.75 (1H, dd, J =8.4, 1.9 Hz), 8.43 (1H, dd, J = 1.9, 0.5 Hz) 88 % yield (Figure S30).

NMR and HR-ESI-MS

All NMR experiments were recorded with a Bruker AVANCE III HD 850 NMR spectrometer with a 5 mm TCI cryoprobe operating at 850 MHz (^{1}H) and 212.5 MHz (^{13}C), with chemical shifts given in ppm (δ) for ^{1}H and ^{13}C NMR analyses and pulse gradient units, capable of producing magnetic field pulsed gradients in the z-direction of 50 G/cm. The NMR measurements have been done with standard BRUKER pulse sequences. The sample temperature was set to 298K, and deuterium oxide (D_2O) and methanol-d_4 (CD_3OD) were used as a solvent. 2D NMR was acquired with a total 2K data point in F2 and 256 data points in F1 and relaxation delay 2s. ROESY experiments were carried out using a mixing time of 700 ms in the phase-sensitive mode. High-resolution-electrospray ionization (HR-ESI) mass spectra were recorded using an Agilent 1290 Infinity II system equipped with a 6545 LC/Q-TOF mass spectrometer (Agilent Technologies).

CaBS.F - Yellow gum; $[\alpha]_D^{25}$ -8.0 (*c* 0.08, MeOH); ^{1}H (850 MHz) and ^{13}C (212.5 MHz) NMR data, see Table S1; HR-ESI-MS (positive-ion mode) *m/z* 1069.4635 $[M + H]^+$ (calcd. for $C_{52}H_{65}N_{10}O_{15}$, 1069.4631) (Figure S31).

The Job plot was performed by the ^{1}H NMR studies of the ligand with varying amounts of calcium ion in CD_3OD-D_2O (3:1). As shown in Figure 4D, the resonance of H11 was upfield shifted as the mole fraction of Ca^{2+} was increased. The change in the NMR signals of H11 with the mole fraction of Ca^{2+} is listed in (Table S2).

Acknowledgments

This research was supported by the MOTIE (Ministry of Trade, Industry, and Energy in Korea, under the Fostering Global Talents for Innovative Growth Program (P0008746) supervised by the Korea Institute for Advancement of Technology (KIAT), the National Research Foundation of Korea (NRF) grant funded by the Korea government (MSIT) (No. 2021R1A4A1033424, 2019R1A5A2027340, 2021R1A2C2007937, and RS-2023-00252972), the Institute for Basic Science (IBS-R015-D1), Korea Institute of Science and Technology (KIST) institutional program (2E31881-22-032 / 2E33301), and the Korea Basic Science Institute (National research Facilities and Equipment Center) grant funded by the Ministry of Education (2022R1A6C101A751). W.F.D. acknowledges support from the NIH (R35 GM122603) and NSF (Awards MCB 2306190 and CLP 2108660).

References

1. I. Yruela, Transition metals in plant photosynthesis. *Metallomics* **5**, 1090-1109 (2013).
2. H. Takala, P. Edlund, J. A. Ihalainen, S. Westenhoff, Tips and turns of bacteriophytochrome photoactivation. *Photochemical & Photobiological Sciences* **19**, 1488-1510 (2020).
3. J. R. Winkler, H. B. Gray, Electron Flow through Metalloproteins. *Chemical Reviews* **114**, 3369-3380 (2014).
4. K. Krzywoszyńska, D. Witkowska, J. Swiatek-Kozlowska, A. Szebesczyk, H. Kozłowski, General Aspects of Metal Ions as Signaling Agents in Health and Disease. *Biomolecules* **10** (2020).
5. J. Liu *et al.*, Metalloproteins Containing Cytochrome, Iron–Sulfur, or Copper Redox Centers. *Chemical Reviews* **114**, 4366-4469 (2014).
6. K. J. Koebke, T. B. J. Pinter, W. C. Pitts, V. L. Pecoraro, Catalysis and Electron Transfer in De Novo Designed Metalloproteins. *Chem Rev* **122**, 12046-12109 (2022).
7. J. Dai *et al.*, Protein-Embedded Metalloporphyrin Arrays Templated by Circularly Permuted Tobacco Mosaic Virus Coat Proteins. *ACS Nano* **15**, 8110-8119 (2021).
8. M. Lella, S. Kamilla, V. Jain, R. Mahalakshmi, Molecular Mechanism of Holin Transmembrane Domain I in Pore Formation and Bacterial Cell Death. *ACS Chem Biol* **11**, 910-920 (2016).
9. M. L. Diss, A. J. Kennan, Heterotrimeric coiled coils with core residue urea side chains. *J Org Chem* **73**, 9752-9755 (2008).
10. S. S. Chaturvedi, D. Bím, C. Z. Christov, A. N. Alexandrova, From random to rational: improving enzyme design through electric fields, second coordination sphere interactions, and conformational dynamics. *Chemical Science* **14**, 10997-11011 (2023).
11. M. Chino *et al.*, Designed Rubredoxin miniature in a fully artificial electron chain triggered by visible light. *Nature Communications* **14**, 2368 (2023).
12. S. I. Mann, A. Nayak, G. T. Gassner, M. J. Therien, W. F. DeGrado, De Novo Design, Solution Characterization, and Crystallographic Structure of an Abiological Mn-Porphyrin-Binding Protein Capable of Stabilizing a Mn(V) Species. *J Am Chem Soc* **143**, 252-259 (2021).
13. N. F. Polizzi *et al.*, De novo design of a hyperstable non-natural protein–ligand complex with sub-Å accuracy. *Nature Chemistry* **9**, 1157-1164 (2017).
14. L. Wang *et al.*, Electron donor-free photoredox catalysis via an electron transfer cascade by cooperative organic photocatalysts. *Catalysis Science & Technology* **8**, 3539-3547 (2018).
15. Q. Ai, S. Pang, K. H. Ahn, Photoswitchable "Turn-on" Fluorescence Diarylethenes: Substituent Effects on Photochemical Properties and Electrochromism. *Chemistry* **22**, 656-662 (2016).
16. A. A. Vasilev, S. Baluschev, S. Ilieva, D. Cheshmedzhieva, E–Z Photoisomerization in Proton-Modulated Photoswitchable Merocyanine Based on Benzothiazolium and o-Hydroxynaphthalene Platform. http://dx.doi.org/10.3390/photochem3020018.
17. A. D. Trowbridge *et al.*, Small molecule photocatalysis enables drug target identification via energy transfer. *Proceedings of the National Academy of Sciences* **119**, e2208077119 (2022).

18. R. J. Mart, R. K. Allemann, Azobenzene photocontrol of peptides and proteins. *Chemical Communications* **52**, 12262-12277 (2016).
19. C. Knie *et al.*, ortho-Fluoroazobenzenes: visible light switches with very long-Lived Z isomers. *Chemistry* **20**, 16492-16501 (2014).
20. B. Schierling *et al.*, Controlling the enzymatic activity of a restriction enzyme by light. *Proc Natl Acad Sci U S A* **107**, 1361-1366 (2010).
21. D. Hoersch, S.-H. Roh, W. Chiu, T. Kortemme, Reprogramming an ATP-driven protein machine into a light-gated nanocage. *Nature Nanotechnology* **8**, 928-932 (2013).
22. S. Kneissl, E. J. Loveridge, C. Williams, M. P. Crump, R. K. Allemann, Photocontrollable peptide-based switches target the anti-apoptotic protein Bcl-xL. *Chembiochem* **9**, 3046-3054 (2008).
23. H. Shishido, M. D. Yamada, K. Kondo, S. Maruta, Photocontrol of calmodulin interaction with target peptides using azobenzene derivative. *J Biochem* **146**, 581-590 (2009).
24. O. I. Lungu *et al.*, Designing photoswitchable peptides using the AsLOV2 domain. *Chem Biol* **19**, 507-517 (2012).
25. A. Pudasaini, K. K. El-Arab, B. D. Zoltowski, LOV-based optogenetic devices: light-driven modules to impart photoregulated control of cellular signaling. *Front Mol Biosci* **2**, 18 (2015).
26. Y. Imamoto, M. Kataoka, Structure and photoreaction of photoactive yellow protein, a structural prototype of the PAS domain superfamily. *Photochem Photobiol* **83**, 40-49 (2007).
27. D. Strickland *et al.*, TULIPs: tunable, light-controlled interacting protein tags for cell biology. *Nat Methods* **9**, 379-384 (2012).
28. Y. I. Wu *et al.*, A genetically encoded photoactivatable Rac controls the motility of living cells. *Nature* **461**, 104-108 (2009).
29. O. Bozovic, B. Jankovic, P. Hamm, Using azobenzene photocontrol to set proteins in motion. *Nat Rev Chem* **6**, 112-124 (2022).
30. R. S. Ritterson, K. M. Kuchenbecker, M. Michalik, T. Kortemme, Design of a photoswitchable cadherin. *J Am Chem Soc* **135**, 12516-12519 (2013).
31. F. Bonardi, G. London, N. Nouwen, B. L. Feringa, A. J. M. Driessen, Light-Induced Control of Protein Translocation by the SecYEG Complex. *Angewandte Chemie International Edition* **49**, 7234-7238 (2010).
32. A. Levskaya, O. D. Weiner, W. A. Lim, C. A. Voigt, Spatiotemporal control of cell signalling using a light-switchable protein interaction. *Nature* **461**, 997-1001 (2009).
33. M. Grusch *et al.*, Spatio-temporally precise activation of engineered receptor tyrosine kinases by light. *Embo j* **33**, 1713-1726 (2014).
34. D. A. James, D. C. Burns, G. A. Woolley, Kinetic characterization of ribonuclease S mutants containing photoisomerizable phenylazophenylalanine residues. *Protein Eng* **14**, 983-991 (2001).
35. C. Carrasco-López *et al.*, Development of light-responsive protein binding in the monobody non-immunoglobulin scaffold. *Nat Commun* **11**, 4045 (2020).
36. A. A. Gil *et al.*, Optogenetic control of protein binding using light-switchable nanobodies. *Nature Communications* **11**, 4044 (2020).
37. L. He, P. Tan, Y. Huang, Y. Zhou, Design of Smart Antibody Mimetics with Photosensitive Switches. *Adv Biol (Weinh)* **5**, e2000541 (2021).

38. J. J. Yi, H. Wang, M. Vilela, G. Danuser, K. M. Hahn, Manipulation of endogenous kinase activity in living cells using photoswitchable inhibitory peptides. *ACS Synth Biol* **3**, 788-795 (2014).
39. D. Schmidt, P. W. Tillberg, F. Chen, E. S. Boyden, A fully genetically encoded protein architecture for optical control of peptide ligand concentration. *Nat Commun* **5**, 3019 (2014).
40. S. Samanta *et al.*, Photoswitching azo compounds in vivo with red light. *J Am Chem Soc* **135**, 9777-9784 (2013).
41. M. J. Kennedy *et al.*, Rapid blue-light-mediated induction of protein interactions in living cells. *Nature methods* **7**, 973-975 (2010).
42. R. M. Woloschuk *et al.*, Structure-based design of a photoswitchable affibody scaffold. *Protein Sci* **30**, 2359-2372 (2021).
43. K. Kimura, T. Yamashita, M. Yokoyama, Syntheses, cation complexation, isomerization and photochemical cation-binding control of spirobenzopyrans carrying a monoazacrown moiety at the 8-position. *Journal of the Chemical Society, Perkin Transactions 2* 10.1039/P29920000613, 613-619 (1992).
44. O. A. Fedorova *et al.*, Effect of metal cations on the photochromic properties of spironaphthoxazines conjugated with aza-15(18)-crown-5(6) ethers. *New Journal of Chemistry* **26**, 1137-1145 (2002).
45. D. Avagliano, S. Tkaczyk, P. A. Sánchez-Murcia, L. González, Enhanced Rigidity Changes Ultraviolet Absorption: Effect of a Merocyanine Binder on G-Quadruplex Photophysics. *J Phys Chem Lett* **11**, 10212-10218 (2020).
46. C. Deo, L. D. Lavis, Synthetic and genetically encoded fluorescent neural activity indicators. *Current Opinion in Neurobiology* **50**, 101-108 (2018).
47. M. Oheim *et al.*, New red-fluorescent calcium indicators for optogenetics, photoactivation and multi-color imaging. *Biochimica et Biophysica Acta (BBA) - Molecular Cell Research* **1843**, 2284-2306 (2014).
48. A. Lewit-Bentley, S. Réty, EF-hand calcium-binding proteins. *Current Opinion in Structural Biology* **10**, 637-643 (2000).
49. M. S. Cates *et al.*, Metal-ion affinity and specificity in EF-hand proteins: coordination geometry and domain plasticity in parvalbumin. *Structure* **7**, 1269-1278 (1999).
50. J. H. Mills *et al.*, Computational Design of an Unnatural Amino Acid Dependent Metalloprotein with Atomic Level Accuracy. *Journal of the American Chemical Society* **135**, 13393-13399 (2013).
51. E. N. Salgado *et al.*, Metal templated design of protein interfaces. *Proceedings of the National Academy of Sciences* **107**, 1827-1832 (2010).
52. G. S. Shaw, R. S. Hodges, B. D. Sykes, Calcium-induced peptide association to form an intact protein domain: 1H NMR structural evidence. *Science* **249**, 280-283 (1990).
53. K. M. Blacklock, B. J. Yachnin, G. A. Woolley, S. D. Khare, Computational Design of a Photocontrolled Cytosine Deaminase. *J Am Chem Soc* **140**, 14-17 (2018).
54. R. L. Rardin *et al.*, Synthesis and Characterization of the Linear Trinuclear Complexes [M(O2CCH3)6(biphme)2], M = Mn, Fe. *Angewandte Chemie International Edition in English* **29**, 812-814 (1990).
55. M. Natali, L. Soldi, S. Giordani, A photoswitchable Zn (II) selective spiropyran-based sensor. *Tetrahedron* **66**, 7612-7617 (2010).

56. F. Fernandez-Belda, Lanthanum as a calcium-substituting ion for binding to sarcoplasmic reticulum ATPase. *Arch Biochem Biophys* **267**, 770-775 (1988).
57. V. Nikolova, N. Kircheva, S. Dobrev, S. Angelova, T. Dudev, Lanthanides as Calcium Mimetic Species in Calcium-Signaling/Buffering Proteins: The Effect of Lanthanide Type on the Ca(2+)/Ln(3+) Competition. *Int J Mol Sci* **24** (2023).
58. D. C. Corson, T. C. Williams, B. D. Sykes, Calcium binding proteins: optical stopped-flow and proton nuclear magnetic resonance studies of the binding of the lanthanide series of metal ions to parvalbumin. *Biochemistry* **22**, 5882-5889 (1983).
59. J. J. Falke, S. K. Drake, A. L. Hazard, O. B. Peersen, Molecular Tuning of Ion Binding to Calcium Signaling Proteins. *Quarterly Reviews of Biophysics* **27**, 219-290 (1994).
60. X. Liu, H. Li, L. Deng, Highly Enantioselective Amination of α-Substituted α-Cyanoacetates with Chiral Catalysts Accessible from Both Quinine and Quinidine. *Organic Letters* **7**, 167-169 (2005).
61. N. Shao *et al.*, Copper Ion-Selective Fluorescent Sensor Based on the Inner Filter Effect Using a Spiropyran Derivative. *Analytical Chemistry* **77**, 7294-7303 (2005).
62. G. Yu *et al.*, A spirobenzopyran-based multifunctional chemosensor for the chromogenic sensing of Cu2+ and fluorescent sensing of hydrazine with practical applications. *Sensors and Actuators B: Chemical* **245**, 803-814 (2017).
63. N. E. Polyakov *et al.*, Complexation of Lappaconitine with Glycyrrhizic Acid: Stability and Reactivity Studies. *The Journal of Physical Chemistry B* **109**, 24526-24530 (2005).
64. S. Xhani *et al.*, Intrinsic disorder controls two functionally distinct dimers of the master transcription factor PU.1. *Sci Adv* **6**, eaay3178 (2020).
65. N. Nandwani *et al.*, A five-residue motif for the design of domain swapping in proteins. *Nature Communications* **10**, 452 (2019).
66. L. Kaltschnee *et al.*, Extraction of distance restraints from pure shift NOE experiments. *J Magn Reson* **271**, 99-109 (2016).
67. S. Kim *et al.*, CHARMM-GUI ligand reader and modeler for CHARMM force field generation of small molecules. *J Comput Chem* **38**, 1879-1886 (2017).
68. R. B. Best *et al.*, Optimization of the Additive CHARMM All-Atom Protein Force Field Targeting Improved Sampling of the Backbone φ, ψ and Side-Chain χ1 and χ2 Dihedral Angles. *Journal of Chemical Theory and Computation* **8**, 3257-3273 (2012).
69. F. F. Liu, Z. Liu, S. Bai, X. Y. Dong, Y. Sun, Exploring the inter-molecular interactions in amyloid-β protofibril with molecular dynamics simulations and molecular mechanics Poisson-Boltzmann surface area free energy calculations. *J Chem Phys* **136**, 145101 (2012).

Figures Legends

Scheme 1. Schematic representation of photoswitchable Ca^{2+}-binding organic-peptide hybrid that reversibly self-associates to form a Ca^{2+}-binding dimer in response to different light wavelengths.

Scheme 2. Synthesis pathway of spiropyran moiety and its conjugation with peptide.

Figure 1. Overview of the computational design of a photoswitchable domain-swapped calcium-binding dimer. calmodulin (PDB: 1CLL) served as the inspiration for the design. The loop from the EF-hand motif (helix-loop-helix) of calmodulin can satisfy five coordination bonds. Glu31 from the neighboring helix was eliminated, and an MC was substituted at this position as a light-switchable ligand. The resulting MC ligand projected away from the Ca^{2+} binding site in the monomeric complex. However, when two EF-loop-MC units were arranged with C2 symmetry, the MC group of one molecule formed a favorable metal-binding site with a symmetry related model (and vice versa) in a domain-swapped model. The domain-swapping interaction completes the coordination sphere of the Ca^{2+} ions; thus, we expect that binding of Ca^{2+} will induce dimerization. The structure was optimized using Rosetta, initially restraining the sidechain and mainchain torsional angles as in 1CLL. The phi/psi angles of the N-terminal Asp20 residue were altered to facilitate the domain-swapping interactions. While optimizing the geometry it became apparent that the C-terminal residue's T26 sidechain could interact with the MC, and this interaction could be enhanced by increasing the bulk of the sidechain to Phe.

Figure 2. MD simulation of designed candidates. (A) Binding energy between Ca^{2+} and peptide candidates. (B) Cosine value distribution between two vectors along the SP molecule and peptide backbone, used to evaluate the geometry C2-symmetric dimers in peptide candidates. The ideal range of cosine values for C2-symmetric dimer is from -0.5 to -1 (Figure S1C and D). (C) Ca^{2+} coordination geometry from MD simulation at the last 100 ns well fitted with designed coordination geometry. (D) Distance between monomer chains with and without calcium. The distance was calculated by determining the center of mass of each peptide chain. The error bars (gray) represent deviation from the mean distance between peptides without Ca^{2+} (blue line) and with Ca^{2+} (red line) from three replicated MD simulations.

Figure 3. Validation of the selectivity and photoactivity of designed candidates. (A) UV/visible spectral analysis of CaBS.F in the presence of La^{3+}, Ca^{2+}, Zn^{2+}, Na^{+}, Cu^{2+}, Co^{2+}, Mn^{2+}, and Mg^{2+} insert picture showing color change and selectivity to calcium ion. The SP form of the peptide is converted to MC (upper row in A) by broad-band UV irradiation. CaBS.F was prepared at 50 μM in phosphate buffered saline (PBS) (pH 7.1, 293 K) and incubated with 1.0 equivalent of the indicated metal ions. (B) The absorbance of CaBS.F upon addition of Ca^{2+} from 0 equivalent to 1.2 equivalent. (C) Emission changes for CaBS.F intensity increase at 510 nm accordingly in PBS buffer. (D) Binding affinity for CaBS.F by titration of Ca^{2+} by UV/visible light. The error bars represent standard deviations from three experimental replicates $n = 3$. (E) Photoswitchable measurement of CaBS.F in the presence of Ca^{2+} by cycling between 365 nm UV light and visible light, monitored at 410 nm.

Figure 4. NMR analysis of the calcium binding site and dimerization of the MC form of CaBS.F driven by calcium ion. (A) Model structure of domain-swapped dimer CaBS.F and calcium binding sites. The atom number of each residue is designated in table S1. (B) HMBC spectra for a range showing the chemical shift of the nearest carbon atom from each bonded oxygen atom without Ca^{2+} (blue) and with Ca^{2+} (red). A clear chemical shift is shown for the CaBS.F's Ca^{2+} binding residues. (C) The Ca^{2+} binding sites of Asp1, Asp3 and Asp5 at the chemical shift of position 4, Phe7 at position 1, and MC at position 14 show clear chemical peak shifts in which these residues cooperate with Ca^{2+} to indicate a binding in the presence of Ca^{2+}. (D) Job's plot for determining the stoichiometry of CaBS.F and Ca^{2+} ions. The error bars represent standard deviations from three experimental replicates $n = 3$. (E) DOSY NMR analysis with the addition of 0~1.5 equivalent of calcium. The diffusion coefficient value decreased upon increasing Ca^{2+}

concentration and saturated at 1 equivalent. The error bars represent standard deviations from three experimental replicates $n = 3$. (F) SEC of the complex shows a clear formational change from monomer to dimeric form.

Figure 5. NMR generated structure of CaBS.F-Ca^{2+} complex from NOE-restrained MD simulations of the calcium-binding site and the domain-swapped dimeric structure. (A) ROESY NMR spectra of CaBS.F + Ca^{2+}. (B) Cluster analysis from structural trajectories at 10 ps. (C) Representative NMR-derived structure from dominant cluster (cyan for peptide and yellow for MC) compared with the designed model (gray).

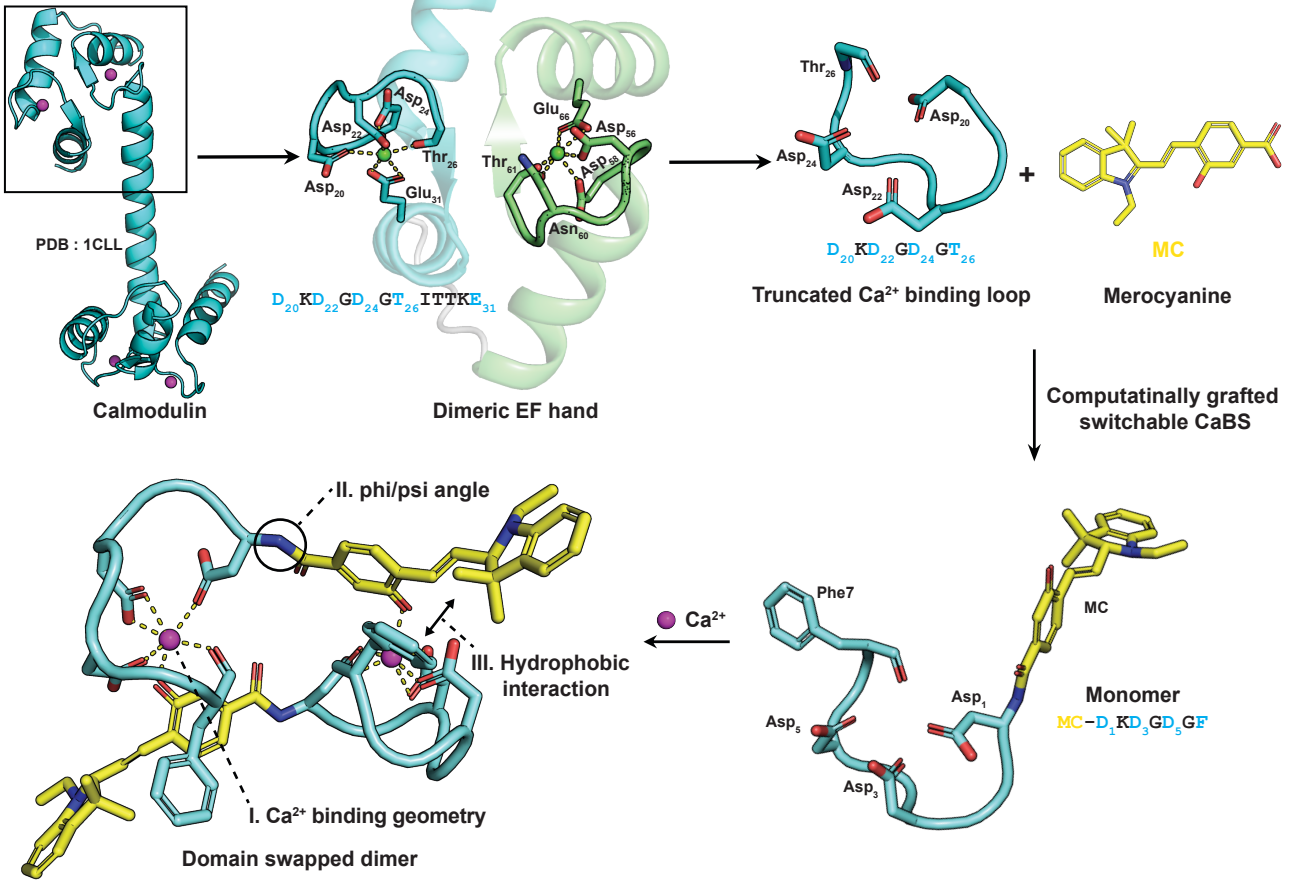
PDB : 1CLL
Calmodulin
Asp24
Asp22
Thr26
Asp20
Glu31
Glu66
Asp56
Thr61
Asp58
Asn60
D20KD22GD24GT26ITTKE31
Dimeric EF hand
Thr26
Asp20
Asp24
Asp22
D20KD22GD24GT26
Truncated Ca2+ binding loop
+
MC
Merocyanine
Computatinally grafted switchable CaBS
Phe7
MC
Asp1
Asp5
Asp3
Monomer
MC–D1KD3GD5GF
Ca2+
II. phi/psi angle
III. Hydrophobic interaction
I. Ca2+ binding geometry
Domain swapped dimer

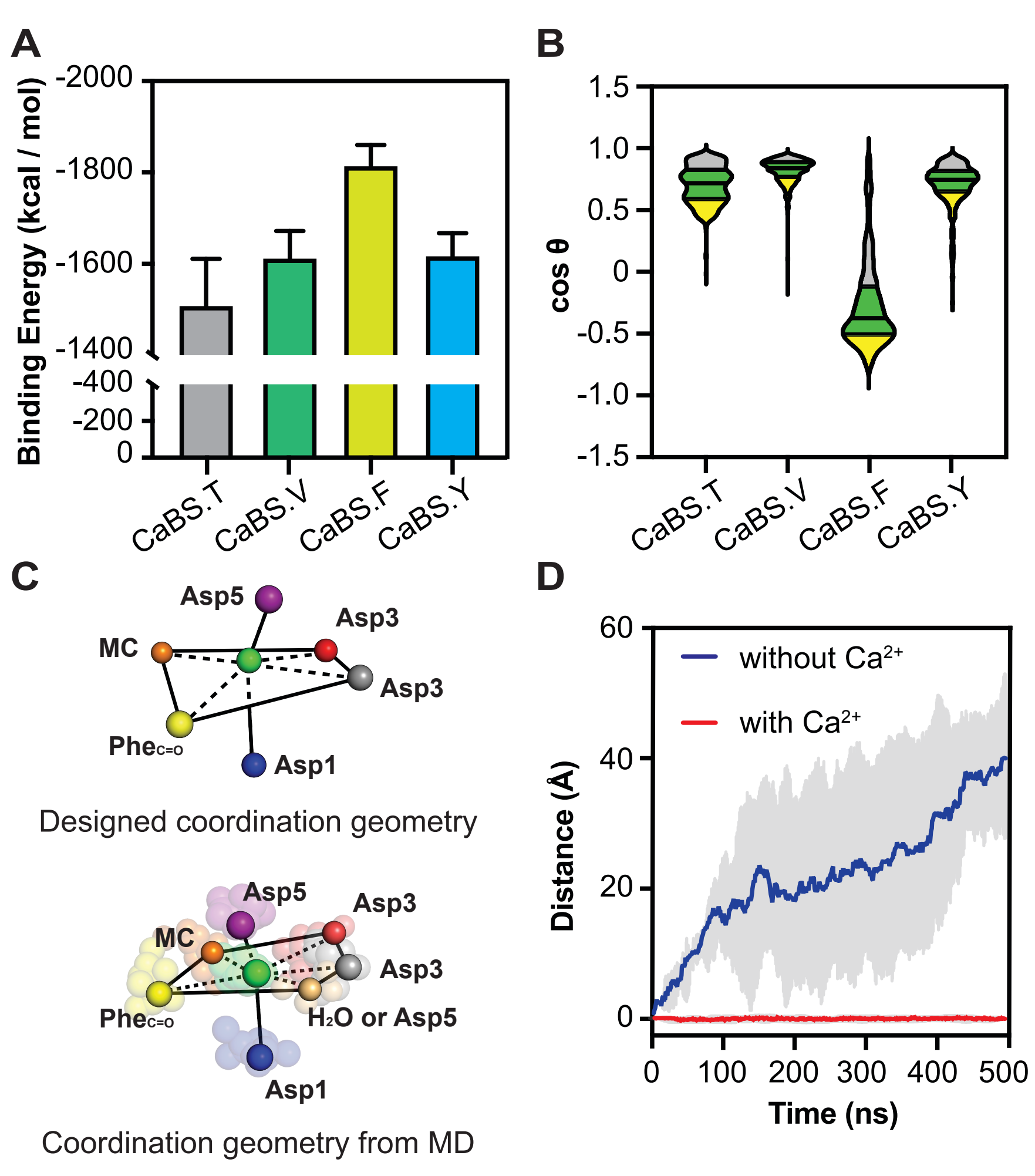
A
Binding Energy (kcal / mol)
-2000
-1800
-1600
-1400
-400
-200
0
CaBS.T
CaBS.V
CaBS.F
CaBS.Y
B
cos θ
1.5
1.0
0.5
0
-0.5
-1.0
-1.5
CaBS.T
CaBS.V
CaBS.F
CaBS.Y
C
Asp5
Asp3
MC
Asp3
Phe$_{C=O}$
Asp1
Designed coordination geometry
Asp5
Asp3
MC
Asp3
Phe$_{C=O}$
H$_2$O or Asp5
Asp1
Coordination geometry from MD
D
Distance (Å)
60
40
20
0
without Ca^{2+}
with Ca^{2+}
0
100
200
300
400
500
Time (ns)

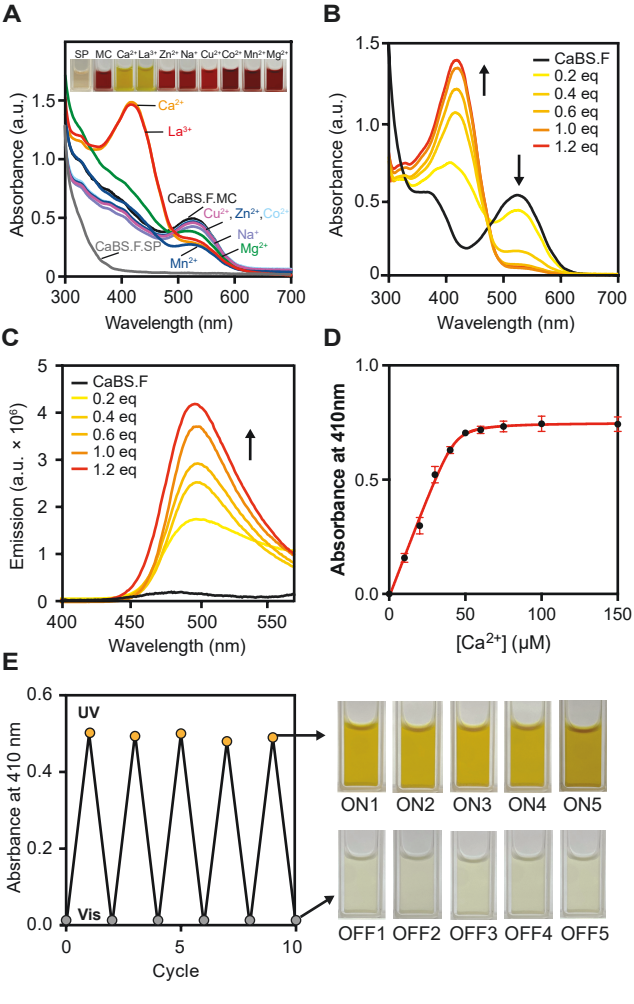
A
SP MC Ca2+ La3+ Zn2+ Na+ Cu2+ Co2+ Mn2+ Mg2+
Ca2+
La3+
CaBS.F.MC
Cu2+, Zn2+, Co2+
Na+
Mg2+
Mn2+
CaBS.F.SP
Absorbance (a.u.)
Wavelength (nm)
B
CaBS.F
0.2 eq
0.4 eq
0.6 eq
1.0 eq
1.2 eq
Absorbance (a.u.)
Wavelength (nm)
C
CaBS.F
0.2 eq
0.4 eq
0.6 eq
1.0 eq
1.2 eq
Emission (a.u. × 10^6)
Wavelength (nm)
D
Absorbance at 410nm
[Ca2+] (μM)
E
UV
Vis
Absrbance at 410 nm
Cycle
ON1 ON2 ON3 ON4 ON5
OFF1 OFF2 OFF3 OFF4 OFF5

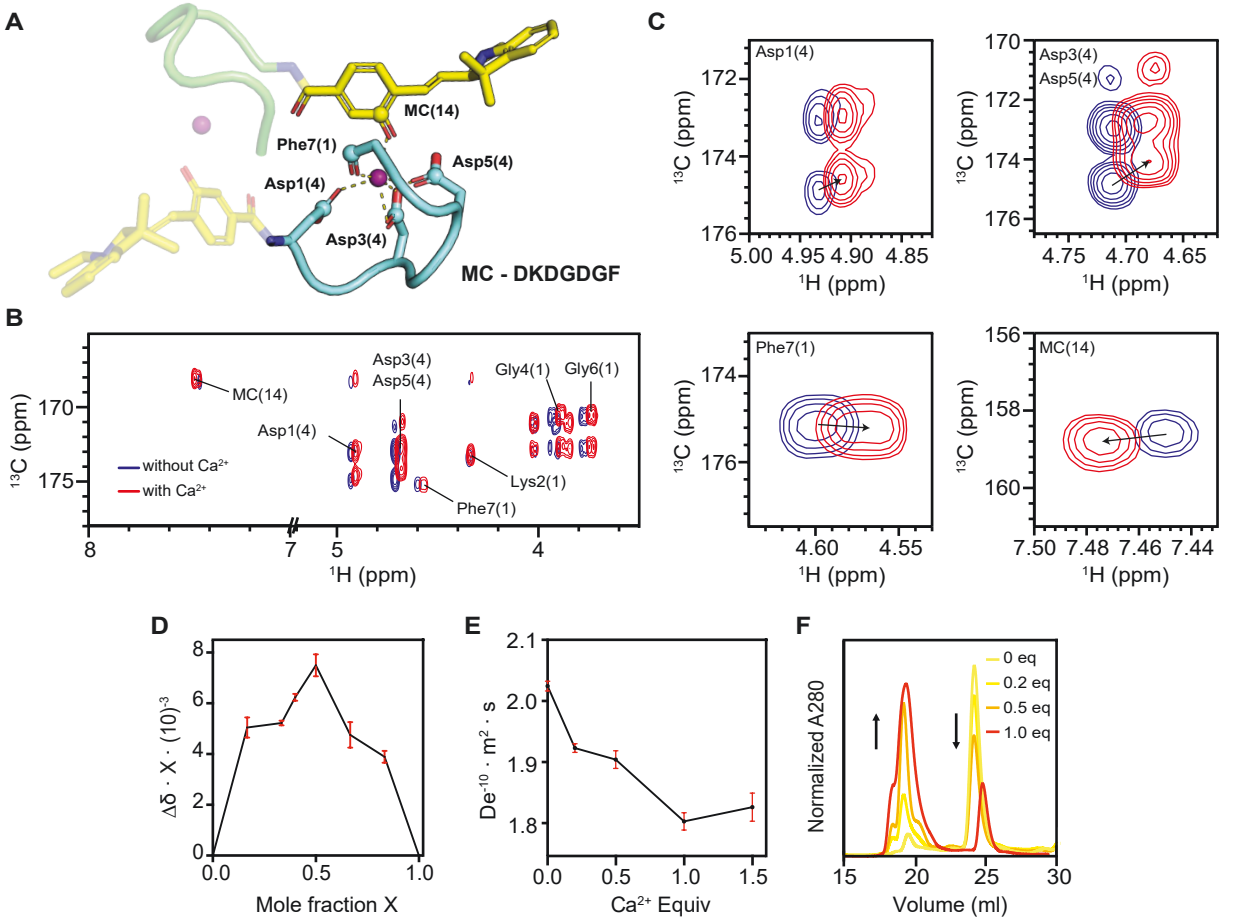
A
MC(14)
Phe7(1)
Asp5(4)
Asp1(4)
Asp3(4)
MC - DKDGDGF
B
MC(14)
Asp3(4)
Asp5(4)
Asp1(4)
Gly4(1)
Gly6(1)
Lys2(1)
Phe7(1)
without Ca2+
with Ca2+
13C (ppm)
1H (ppm)
C
Asp1(4)
Asp3(4)
Asp5(4)
Phe7(1)
MC(14)
13C (ppm)
1H (ppm)
D
Δδ · X · (10)-3
Mole fraction X
E
De-10 · m2 · s
Ca2+ Equiv
F
0 eq
0.2 eq
0.5 eq
1.0 eq
Normalized A280
Volume (ml)

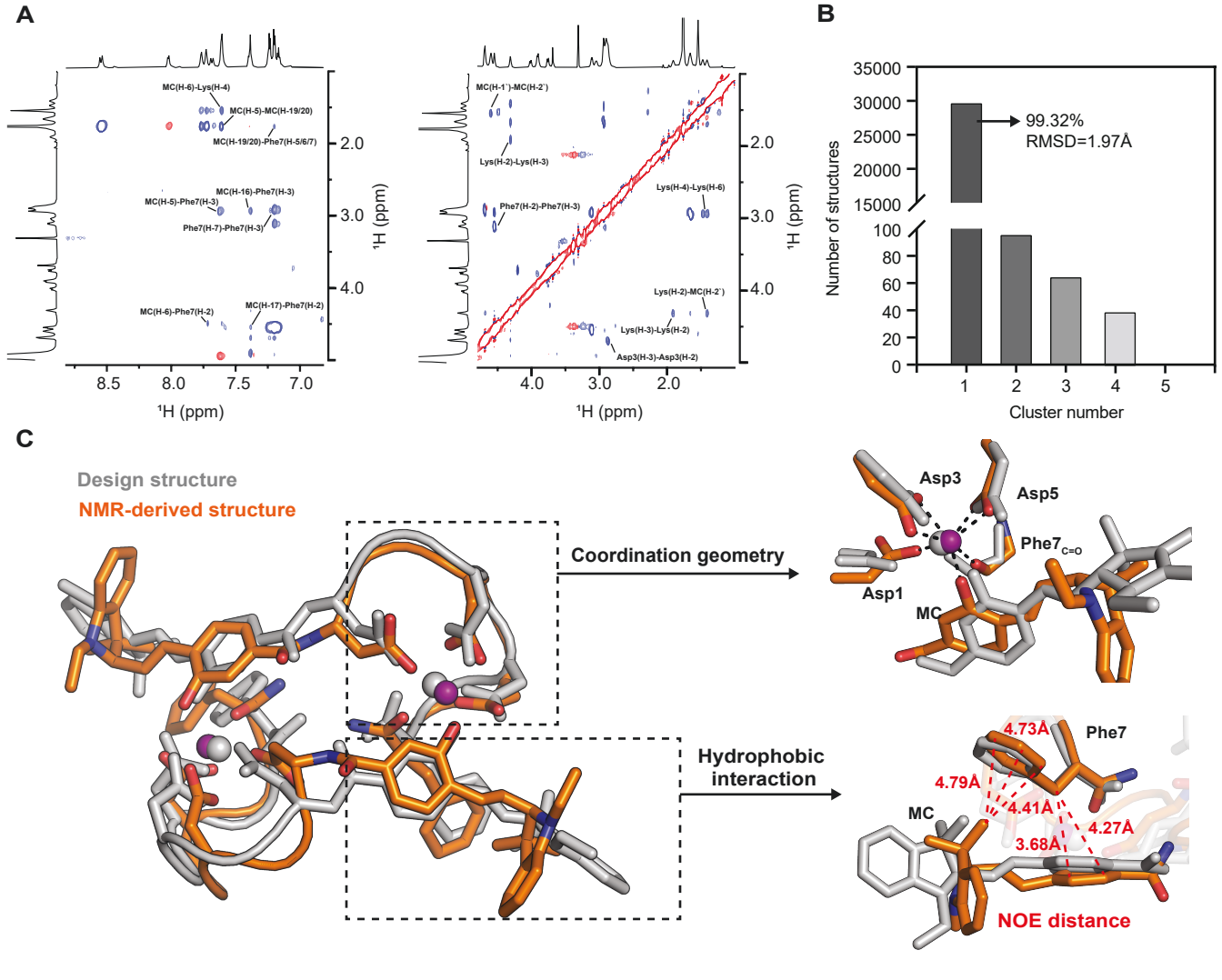
A
MC(H-6)-Lys(H-4)
MC(H-5)-MC(H-19/20)
MC(H-19/20)-Phe7(H-5/6/7)
MC(H-16)-Phe7(H-3)
MC(H-5)-Phe7(H-3)
Phe7(H-7)-Phe7(H-3)
MC(H-6)-Phe7(H-2)
MC(H-17)-Phe7(H-2)
MC(H-1')-MC(H-2')
Lys(H-2)-Lys(H-3)
Phe7(H-2)-Phe7(H-3)
Lys(H-4)-Lys(H-6)
Lys(H-2)-MC(H-2')
Lys(H-3)-Lys(H-2)
Asp3(H-3)-Asp3(H-2)
¹H (ppm)
B
Number of structures
99.32%
RMSD=1.97Å
Cluster number
C
Design structure
NMR-derived structure
Coordination geometry
Asp3
Asp5
Phe7C=O
Asp1
MC
Hydrophobic interaction
Phe7
4.73Å
4.79Å
4.41Å
4.27Å
3.68Å
MC
NOE distance

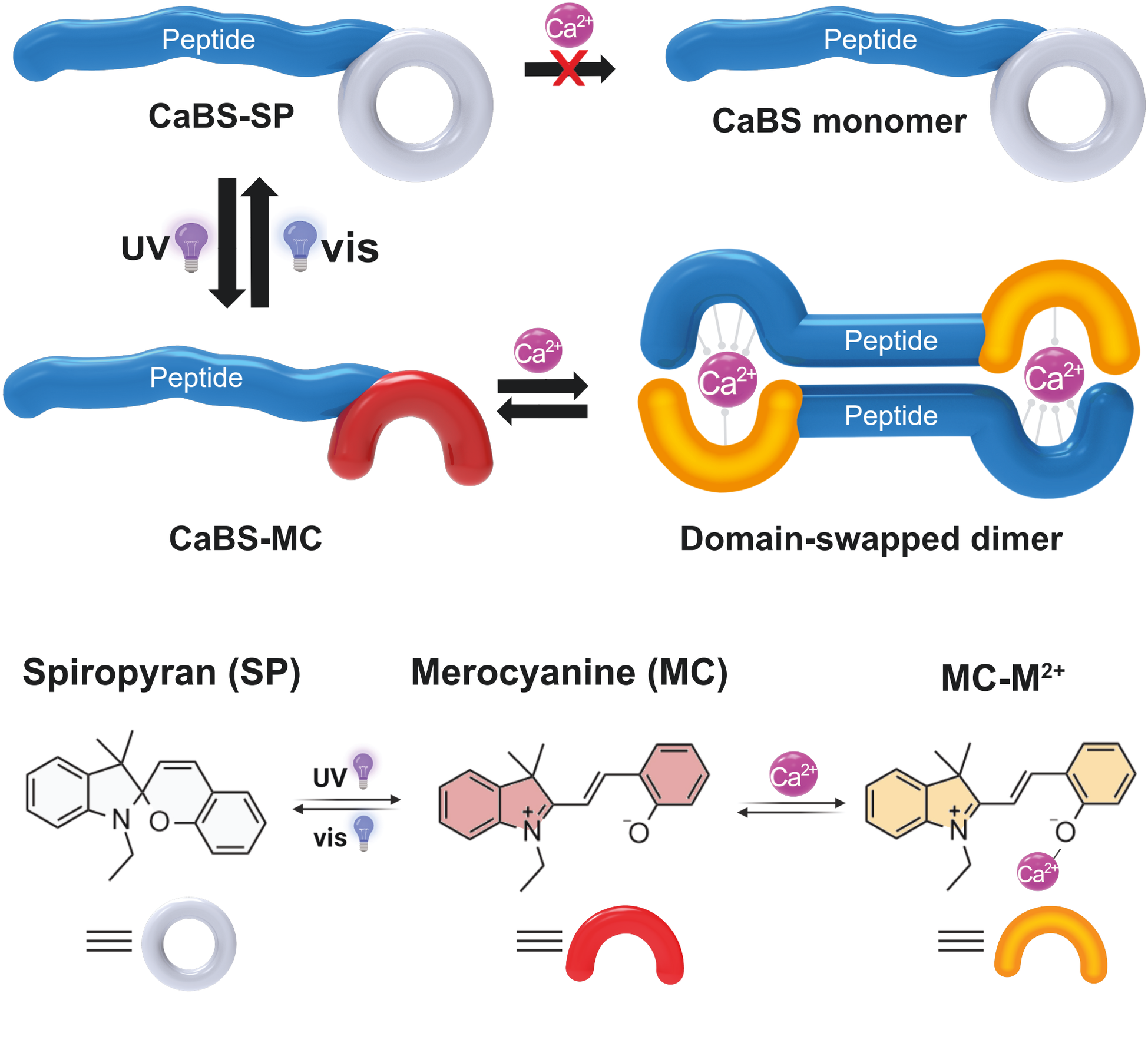
Peptide
CaBS-SP
Ca2+
Peptide
CaBS monomer
UV
vis
Peptide
CaBS-MC
Ca2+
Peptide
Peptide
Ca2+
Ca2+
Domain-swapped dimer
Spiropyran (SP)
Merocyanine (MC)
MC-M2+
UV
vis
N
O
Ca2+

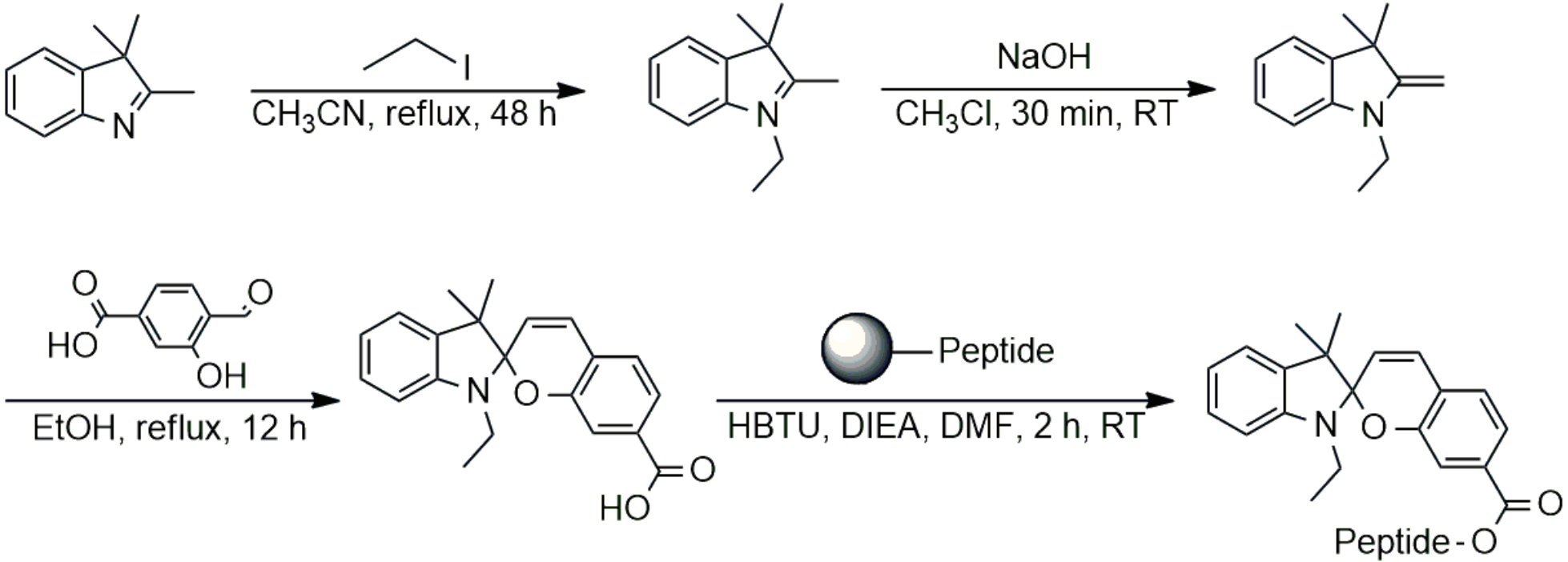
I
CH3CN, reflux, 48 h
NaOH
CH3Cl, 30 min, RT
HO
O
OH
EtOH, reflux, 12 h
Peptide
HBTU, DIEA, DMF, 2 h, RT
Peptide - O